Optical Engineering

OpticalEngineering.SPIEDigitalLibrary.org

Advanced environmental control as a key component in the development of ultrahigh accuracy *ex situ* metrology for x-ray optics

Valeriy V. Yashchuk
Nikolay A. Artemiev
Ian Lacey
Wayne R. McKinney
Howard A. Padmore

SPIE.

Advanced environmental control as a key component in the development of ultrahigh accuracy *ex situ* metrology for x-ray optics

Valeriy V. Yashchuk,* Nikolay A. Artemiev, Ian Lacey, Wayne R. McKinney, and Howard A. Padmore
Lawrence Berkeley National Laboratory, Advanced Light Source, Berkeley, California 94720, United States

Abstract. The advent of fully coherent free-electron laser and diffraction-limited synchrotron radiation storage ring sources of x-rays is catalyzing the development of new ultrahigh accuracy metrology methods. To fully exploit these sources, metrology needs to be capable of determining the figure of an optical element with sub-nanometer height accuracy. The major limiting factors of the current absolute accuracy of *ex situ* metrology are drift errors due to temporal instabilities of the lab's environmental conditions and systematic errors inherent to the metrology instruments. Here, we discuss in detail work at the Advanced Light Source X-Ray Optics Laboratory on building of advanced environmental control that is a key component in the development of ultrahigh accuracy *ex situ* metrology for x-ray optics. By a few examples, we show how the improvement of the environmental conditions in the lab allows us to significantly gain efficiency in performing *ex situ* metrology with high-quality x-ray mirrors. The developed concepts and approaches, included in the design of the new X-Ray Optics Laboratory, are described in detail. These data are essential for construction and successful operation of a modern metrology facility for x-ray optics, as well as high-precision measurements in many fields of experimental physics. [DOI: 10.1117/1.OE.54.10.104104]

Keywords: x-ray optics; optical metrology; surface slope profilometry; surface interferometry; microscopy; error reduction; calibration.
Paper 150496P received Apr. 16, 2015; accepted for publication Sep. 10, 2015; published online Oct. 12, 2015.

1 Introduction

Recent progress in electron accelerator technology has inspired synchrotron x-ray facilities around the world to develop plans for the construction of new and upgraded light sources with brightness 2 to 3 orders of magnitude higher than today. In the soft x-ray energy region, less than 2 keV, these sources will have full transverse coherence (see, for example, review articles in Ref. 1). These diffraction limited storage rings (DLSRs) will enable dramatic improvements in many areas of x-ray science, especially for experiments that directly rely on high brightness and high transverse coherence of x-ray beams.[1–4]

Exploitation of the full potential of DLSRs and free-electron laser (FEL) facilities requires near-perfect optics, capable of delivering light to experiments without significant degradation of brightness and coherence, under the high-power operational conditions experienced in beamlines.[1,5,6] The desired quality of the optics (including significantly curved ones) can be illustrated by the residual (after subtraction of an ideal shape) surface slope and height errors of $\sigma_s < 30 - 50$ nrad [root-mean-square (rms)] and $\sigma_h < 0.5 - 1$ nm (rms), respectively.[7–11]

We should note here that for the trustworthy specification of surface quality of x-ray optics for coherent sources, such as DLSRs and FELs, more rigorous consideration is needed because the light distribution in the image depends not only on the averaged (rms) parameters of the imperfection (σ_h and σ_s) but also on the correlation properties of the figure error.[12,13]

In any case, the key to achieving the required high-quality optical systems is metrology;[14–17] and the metrology accuracy has to be a few times better than the required x-ray optical quality.

Optical quality is directly linked to the accuracy of the metrology used in fabrication. For example, combination of very unique fabrication and metrology technologies, elastic emission machining,[18] microstitching interferometry,[19] and relative-angle determinable stitching interferometry,[20] developed by Osaka University, has allowed fabrication of free-shaped x-ray mirrors with relatively small curvature with slope error <0.1 μrad rms and shape error <2 nm peak-to-valley, capable of sub 10-nm diffraction limited focusing.[21]

In spite of remarkable achievements (for review, see Ref. 17 and references therein), the current accuracy of the metrology of x-ray optics, available at the most of x-ray facilities, is still far below today's challenges. The major limiting factors are still the same: drift errors of the measurements due to temporal instabilities and systematic errors inherent to the metrology instruments. Both are very tightly dependent on the laboratory's environmental conditions.

In the present article, we discuss in detail work at the Advanced Light Source (ALS) X-Ray Optics Laboratory (XROL) on building of advanced environmental control that is a key component in the development of ultrahigh accuracy *ex situ* metrology for x-ray optics. On a few examples, we show how the improvement of the environmental conditions in the lab allows us to significantly gain efficiency

*Address all correspondence to: Valeriy V. Yashchuk, E-mail: VVYashchuk@lbl.gov

in performing *ex situ* metrology with high-quality x-ray mirrors. The developed concepts and approaches, included in the design of the new XROL, are described in detail. Due to careful design, the new lab is a cleanroom facility better than Class 500 with a diurnal temperature stability better than ± 30 mK, despite the relatively low construction budget. We believe that our experience in lab design and organization, along with metrology procedures developed and discussed in this paper, are essential for construction and successful operation of a modern metrology facility for x-ray optics, as well as high-precision measurements in many fields of experimental physics.

The paper is organized as follows: in Sec. 2, we formulate requirements for the environmental conditions needed for high accuracy x-ray optics metrology and present design approaches and arrangement of the XROL, recently built at the ALS. In Sec. 3, we describe the measurement capabilities and applications of the main metrology instrumentation, available in the XROL. In Sec. 4 with the example of slope measurements with the developmental long trace profiler (DLTP), we demonstrate the improvements in performance of *ex situ* metrology due to the advanced environmental conditions in the new lab. We conclude in Sec. 5 by summarizing the main results of the work, discussed throughout the paper and essential for successful operation of a modern metrology facility for x-ray optics commensurate with the challenges set by new ultrahigh brightness x-ray sources. In the conclusion, we also briefly outline our plans for instrumentation upgrades and research and development that are inseparable part of the ALS program on radical improvement of x-ray optical metrology.

2 Design and Arrangement of the Advanced Light Source X-Ray Optics Laboratory

2.1 *General Requirements to the Design and Arrangement of a Metrology Laboratory for X-Ray Optics*

There are five major environmental factors that critically affect the performance of *ex situ* (laboratory) metrology tools for x-ray optics. These are (i) temperature stability in the lab, (ii) air convection and turbulence, (iii) air cleanness, (iv) atmospheric pressure and humidity, and (v) vibrations. Because achieving these factors simultaneously may be significantly contradictory, the design of an optical metrology laboratory is always a result of some reasonable compromises.

The scale of errors due to temporal drifts and fluctuations in measurement instrument and experimental set-up strongly depends on the stability and uniformity of temperature over the set-up. The required temperature stability is on the level of a few millikelvins.[16] The limiting factors for temperature stability achievable are the air exchange rate allowable from the point of view of air turbulence and cleanness, and the value and distribution of the heat from different sources, irremovable from the lab, including the instruments, instrumental electronics, and data acquisition and control (DAC) systems. Additionally, because of the typically very long time (many hours) of some measurements (for example, high accuracy surface slope profiling[22,23] and interferometric surface mapping with stitching[20,24]), we are interested in a characteristic time for stability of hours and even days. Practically, cost consideration forces one to specify the temperature stability in the cleanroom space to be on the level of ± 0.1 K/day with minimal periodic temperature variation that usually appears due to a switch-on/switch-off mode of operation of air-conditioning units. In this case, implementation of additional one or two layer enclosures around the measurement set-up provides the required temperature stability on the level of a few millikelvins.[25,26]

Differing from contact measuring systems, metrology instruments employing noncontact optical sensors are extremely sensitive to air turbulence and convection.[27] In this respect, designing as uniform as possible distribution of supply and return air with laminar air flow conditions inside the lab is very important. An example of a design close to the ideal one is the Class 100 cleanroom laboratory of the Clean Room Center at the Physikalisch-Technische Bundesanstalt (PTB), Germany.[28] In the laboratory, almost ideal laminar air flow conditions are achieved due to the strongly vertical direction of the flow supplied through the entire area of the lab ceiling and exhausted through the entire floor area. Behind the perforated flow panels, there is a grid of cylindrical shafts through the concrete floor that are used to uniformly exhaust the air to the basement space. The heat released by laboratory instruments and their electronics is directly exhausted to the basement space. This provides very small temperature gradients. Differing from the majority of optical laboratories around the world, all the precision instrumentation is used without surrounding hutches. This is, in particular, true for the precision angular comparator set-up used for high accuracy calibration of electronic autocollimators (ACs), widely used in surface deflectometry.[25,26,29,30]

When a metrology laboratory is developed in an existing building (the case of the ALS XROL), it is very difficult to ensure the desired high uniformity and laminarity of air flow in the lab. This is because of the necessity to provide both supply and return air through significantly localized intake and exhaust system. Together with the usual restriction set by available funding, this makes it practically impossible to put in place a construction specification for an optical metrology lab for x-ray optics with a cleanroom grade better than Class 10,000. A Class 10,000 cleanroom was formally specified in the construction documentation for the ALS XROL. Below, we demonstrate that with some design, construction, and operational precautions, it is still possible to routinely maintain XROL working conditions to be significantly less than 500 particles/ft^3.

Variations of atmospheric temperature, pressure, humidity, and density of carbon dioxide in the lab affect the value of the air refractive index to a greater or lesser extent.[31,32] Variation of the refractive index directly contributes to the absolute error and reproducibility of almost all optical measurements in air, including distance measuring and surface profiling interferometry. Among these four, the humidity is the less stringent factor. However, even though humidity has a small effect on refractive index, changes in humidity can significantly modify material properties, including shape. Relative humidity changes have been found to be a major factor that decreases long-term measurement reproducibility in a Fizeau interferometer.[33] In a 6-in. aperture interferometer, a relative humidity change of a few dozen percent causes a systematic error due to a nanometer level change of the shape of the instrumental

reference flat. The authors interpret the observation as being a change in the film stress in an antireflective coating on the reverse side of the reference flat due to the adsorption of water molecules.

Addition to the lab specification of a requirement for humidity control knowingly raises the cost of the dedicated climatic system and complicates the operational procedures in the lab. Forgiveness for ignoring humidity control comes from the common property of cleanroom air conditioning to effectively dry the air, decreasing long-term variation of the relative humidity in the cleanroom.

All metrology instruments used for characterization of x-ray optics are very sensitive to vibration. Significantly, in our case, the lab's foundation provides the required stability regarding vibration. Preferably, the foundation has to be a separate monolithic plate of concrete with thickness of 30 to 40 cm or even more. The lab should be placed reasonably close to the facility's experimental floor with easy access to the beamlines (without passing streets, roads, stairs, or elevators). Placing the lab directly on the experimental floor's slab generally leads to an increased level of vibration due to main floor technological activity, such as crane movements. Vibrating and noise-producing lab equipment, such as air-conditioning systems, compressors for optical tables, compressed air dryers, is ideally located in a dedicated technological (mechanical) room, adjacent to the cleanroom lab, but vibrationally and acoustically insulated. The equipment in the mechanical room should be mounted with proper vibration and sound insulation.

2.2 *Space Arrangement of the New Advanced Light Source X-Ray Optics Laboratory*

Figure 1 shows a graphical sketch of the space arrangement of the new X-Ray Optics Laboratory at the ALS. The laboratory space is split into four separated technological rooms: a mechanical room, a control room, a gowning room, and a cleanroom optical metrology laboratory.

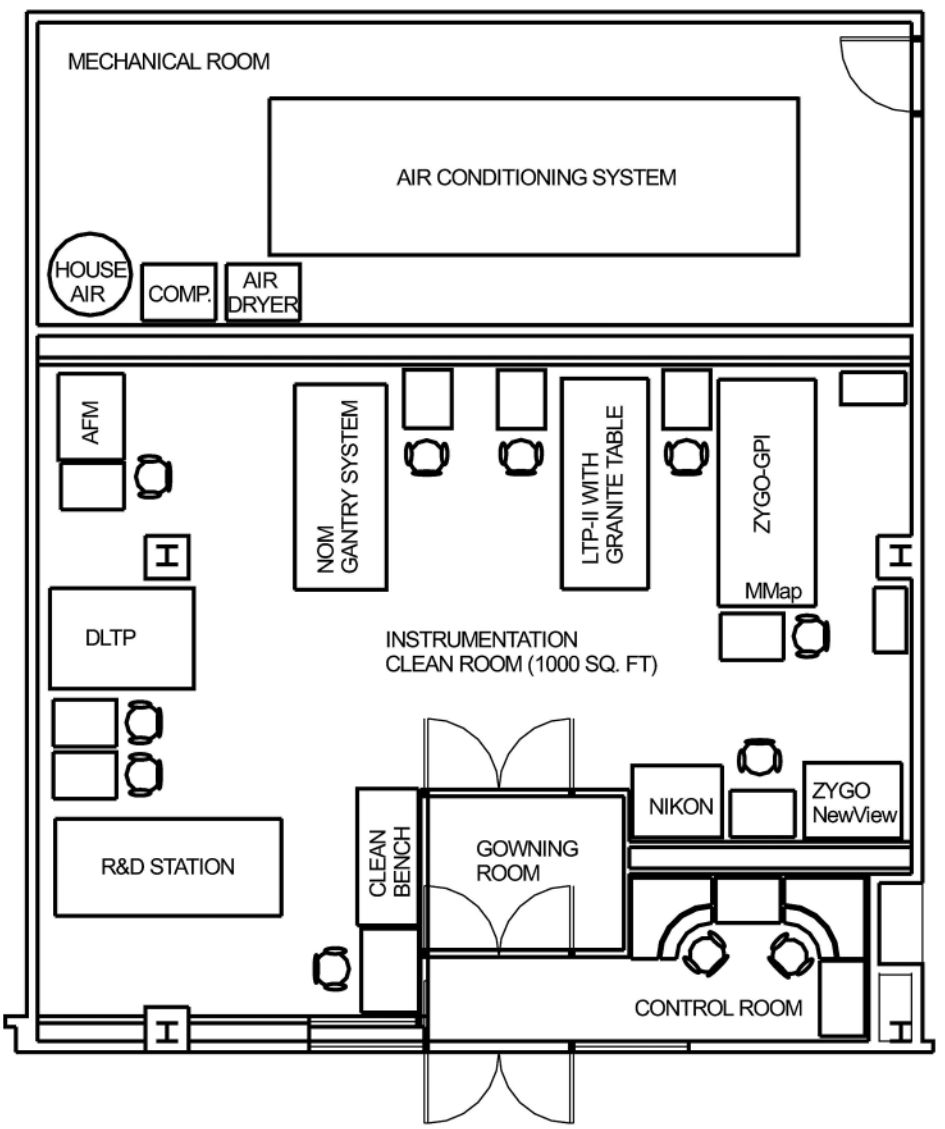

Fig. 1 Floor plan of the Advanced Light Source (ALS) X-Ray Optics Laboratory (XROL), including a cleanroom metrology laboratory (see also Fig. 2), a gowning room, a control room, and a mechanical room. The lab entrance is from the user support building hall used for assembly of set-ups.

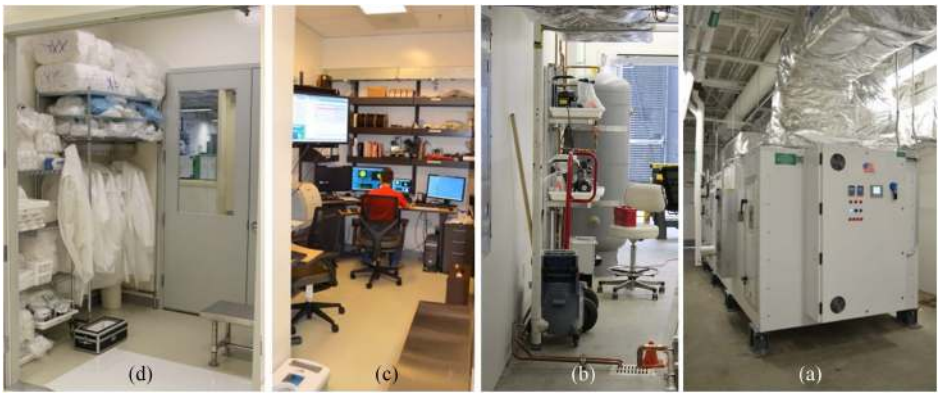

Fig. 2 XROL at the ALS: mechanical room with (a) air conditioning system and (b) air compressors, air dryer, and a 200-l reservoir tank; (c) control room; and (d) gowning room.

The mechanical room [see Figs. 1, 2(a), and 2(b)] accommodates an air-conditioning system, two air compressors for optical tables, an air dryer, and a 200-liter reservoir tank. The last two items are connected to the pressurized ALS house air, supplying air-bearing translation systems of metrology instruments, such as the ALS long trace profiler (LTP)-II[34] and DLTP.[35] Excellent sound insulation of the cleanroom lab from the noise produced by the equipment in the mechanical room is provided with an additional wall, constructed to arrange a high conductivity return air plenum (Fig. 1). The mechanical room with a door to the user support building (USB) lobby has no direct access to the cleanroom laboratory space.

The newly constructed laboratory space is divided into a control room [Fig. 2(c)], a gowning room [Fig. 2(d)], and an instrumentation cleanroom laboratory (Fig. 3).

The control room [Fig. 2(c)] has a number of computer workstations; some of them are dedicated to remote control measurements with instrumentation in the clean room, while the others are used to process, analyze, and archive the measured data. A separate workstation, integrated to the LBNL environmental control network, is used to monitor and optimally tune the XROL air conditioning system.

A buffer zone between the control room and the cleanroom laboratory is arranged as a gowning room. The space in the gowning room is partially used for storage of spare cleanroom clothing and supplies. With the same air conditioning system, the gowning room is over-pressured with respect to the control room that is at normal atmospheric pressure. In its turn, the cleanroom is over-pressured compared to the gowning room. The gowning room is also equipped with a nitrogen blow-off post with a quick disconnect adapter, used for blowing dust off entering components and tools.

Besides the assigned missions, the gowning and control room areas also act as very important temperature buffer zones between the ALS USB assembly hall and the cleanroom lab. With such a spatial arrangement, the XROL additionally benefits from protection offered by the ALS USB environmental control system, subject to the ambient humidity and temperature variations inside the building that are significantly smaller than that of outside air (Sec. 2.3).

2.3 *Design, Arrangement, and Environmental Conditions of the X-Ray Optics Laboratory Cleanroom Metrology Lab*

Figure 3 depicts the overall arrangement of the XROL cleanroom laboratory of about 1000 square feet and the lab's metrology instrumentation. As seen in Fig. 1, access to the lab is made through a gowning room and a small entering hallway of the control room, both with sticky cleanroom entrance mats in heavy traffic floor areas in the front of the doors, helping to maintain cleanroom conditions in the lab.

Table 1 summarizes the major construction specifications of the environmental and operational conditions practically

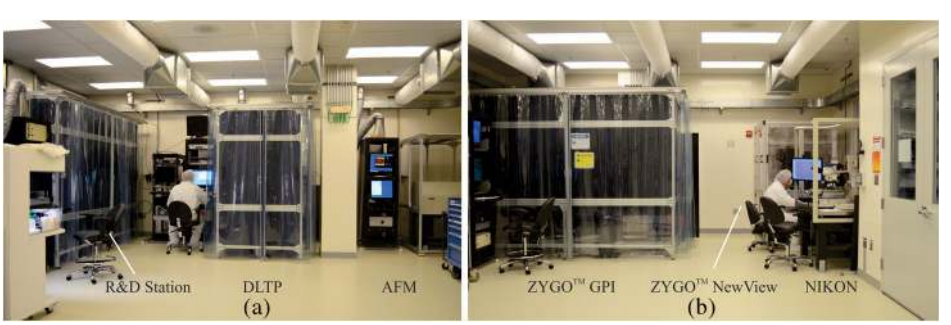

Fig. 3 Lab arrangement and metrology instrumentation in the ALS XROL cleanroom: (a) R&D Station, developmental long trace profiler (DLTP), and atomic force microscope, Veeco™ Dimension-3100, and (b) 6-in. aperture Fizeau interferometer, ZYGO™ GPI, interferometric microscope, ZYGO™ NewView-7300, and an optical microscope, NIKON™ MM-800/L. The second interferometric microscope, MicroMap™-570, is placed on the ZYGO™ GPI optical table. The NOM-like gantry system and the LTP-II with granite table are not depicted here.

Table 1 The construction specifications and the actual operational conditions in the Advanced Light Source (ALS) X-Ray Optics Laboratory.

Environmental control		Specified	Achieved	Comments
Particulate control (particles/ft^3)		Class 10,000	Class < 500	See Fig. 4
Temperature variation at $T_0 = 69.8$ F		±0.25 F	±0.06 F	See Sec. 4
Relative humidity			~45% ± 3.5%	Control not specified; see Fig. 5
Air pressure control	Control room	Ambient at the ALS USB, P_0		
	Gowning room	$P_1 > P_0$, $P_1 - P_0 \approx 80$ μbar		Absolute stabilization not specified
	Cleanroom lab	$P_2 > P_1 > P_0$, $P_2 - P_1 \approx 80$ μbar		Absolute stabilization not specified

achieved in the XROL, after completion of the construction work and moving and recommissioning of the instrumentation shown in Fig. 3.

The construction specifications in Table 1 were limited by the funding available for the construction. Significantly improved operational conditions became possible due to additional requirements to the construction design, materials, and the work procedure, as well as due to a careful specification of the custom air-handler unit and feedback sensors, and cautious procedural control of the everyday lab operation. A review of different design approaches to cleanrooms is presented, for example, in Ref. 36.

The XROL air-conditioning system [Fig. 2(a)], intended to support a Class 10,000 (ISO 7/M 5.5) cleanroom arrangement, is designed to provide a recirculation air change rate (ACR) of ~(30 to 80) air changes/h. Optimization of the ACR within the entire ISO recommended range is possible with the used recirculation air system with variable speed DC fans, smoothly controlled by the lab environmental control work station. There are two preset modes of operation. A maintenance mode with a higher ACR of ~80 air changes/h is designed for the tasks of equipment maintenance, optical alignment, or transfer of optics into the lab or onto an instrument, when human occupants are the primary source of contamination. Once the cleanroom is vacated and measurements are in progress, a measurement mode with a lower ACR of ~30 air changes/h is possible. The latter option was envisaged to minimize the spurious effects of air turbulence on measurements.

The recirculation of air is the most important factor in contamination control of a cleanroom. The recommended design ranges for Class 100 (ISO 5) cleanroom ACRs are from 240 to 480 air changes/h and for Class 1000 (ISO 6) cleanroom ACRs from 150 to 240 air changes/h.[37] Actually, the lower airflow probably even improves the actual cleanliness by minimizing turbulence. Indeed, the operational particle contamination, achieved in the XROL at ACR ≈ 80 air changes/h is much better than Class 1000; see Fig. 4. Figure 4 depicts the particle count in the XROL, recorded with a Fluke particle counter during a period from the middle of September 2013, when the main construction work was completed, through January 2014, when moving, anchoring, and recommissioning of the lab instruments were completed, up to the middle of July 2014. The latter period, with particle contamination below 200 to 300 particles/ft^3, corresponds to normal operation of the lab.

We believe that the advanced particulate control became possible also due to the installation of a grounded (antistatic) style floor, improved cleanroom painting of the ceiling and walls, and careful sealing of all wall and ceiling panel joints, electrical switchers and plugs, communication boxes, etc. Along with physical prevention of dusting with the positive air pressure arrangement (see Table 1), procedural controls, such as usage of higher-grade cleanroom clothing and regular (once a week) cleaning, are also very important to keep the lab clean.

The relatively low recirculation ACR helps to keep inlet airflow conditions close to laminar flow. Additionally, in order to support laminar airflow, we use four long fabric ducts, seen in Fig. 3. The fabric ducting is well suited for very uniform distribution of inlet air. It also prevents transmission of noise from the air handler unit. For providing laminar return flow, the lab design consists of large-area low-wall return grilles and high conductivity return air plenums (Fig. 1).

Hutches and curtain systems, surrounding the metrology instruments (Fig. 3) ameliorate any potential perturbative effect from the inlet airflow to the measurements even at the higher ACR mode. As a result, we are able to routinely

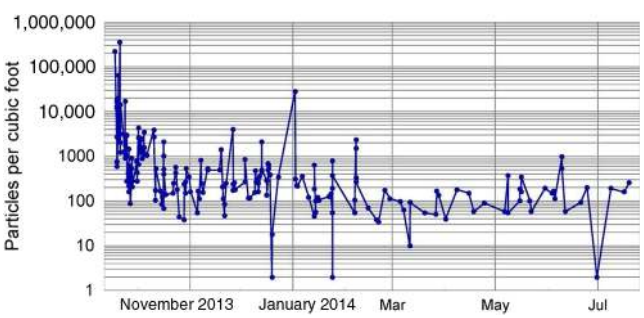

Fig. 4 Particle counts in the XROL from the middle of September 2013 through the middle of July 2014. The major construction work was completed by the middle of September 2013. The instrumentation moving, anchoring, and recommissioning processes were completed in January 2014. The particle contamination below 200 to 300 particles/ft^3 corresponds to a normal operation of the lab. Beginning of 2014, once the XROL air conditioning system was restarted after the holiday shutdown, the peaks of particle contamination, above 1000 coincide with the delivery of large mirror assemblies to be characterized. The drops of the particle contamination to a few particles/ft^3 correspond to the measurements on the lab clean bench with the bench blower activated. The bench is used for handling and assembling optics.

operate the lab in the higher ACR mode, keeping the lab at as low as possible particle contamination.

The temperature stabilization method, realized in the XROL air conditioning system [Fig. 2(a)], consists of two steps. At the first step, the air is cooled down to ~14°C with a water chiller utilizing the building low conductivity water. The desired air temperature and its stability are achieved by resistive heating of the preliminarily cooled air. The current through the dedicated electric trim heating coil is supplied via a silicon-controlled rectifier. This allows smooth feedback control, with very small amplitude of oscillation, for the lab temperature. Besides the advanced design of the air conditioning system, the improved temperature stability (Table 1) and very low level of temperature gradients in the XROL cleanroom lab were achieved due to: (i) minimization of the heat load with connection of the instrumental and DAC electronic racks to 6-in heat exhaust outlets (Fig. 3), (ii) use of feedback temperature sensors with highest available resolution, (iii) heat protection offered by the building environmental control system, and (iv) minimization of human traffic via remote control for the measurements. As a result, the room's temperature stability, measured with three temperature sensors mounted at different positions on the lab walls, is about ±30 mK/day with an ~5-min periodic oscillation. The oscillation was found to be unavoidable due to an operation peculiarity of the computer control feedback system. As shown in Sec. 3, this oscillation does not affect high-sensitivity metrology with our surface slope measuring instrument DLTP that is extremely sensitive to temperature instabilities and gradients around the measuring set-up.

The two-step temperature stabilization realized in the air conditioning system results in effective drying of the lab air. Another important factor, decreasing the lab's air relative humidity variation, is the mode of air recirculation, when about 90% of return air is supplied back into the lab. The humidity stability in the XROL also benefits from the lab's location inside the ALS USB and protection offered by the building's environmental control system.

Figure 5(a) illustrates the variation of the lab air relative humidity during 2 weeks in June 2014. This time is well known in the Bay Area to have strong morning and evening fog. Due to the fog and close distance from the ALS to the San Francisco Bay and Pacific Ocean, the outside humidity varied by almost 70% [Fig. 5(b)]. Nevertheless, the rms variation of the lab humidity was only about 3.5%.

Floor vibration in the new lab was tested in the course of selection of the lab space. The results of the tests were compared with the vibration level in the old metrology lab that was known to be completely acceptable for all metrology instrumentation in use. It was found that in the both spaces, the vibration level is almost the same and does not exceed vibration criterion (VC) curve for vibration-sensitive equipment, VC-E,[38,39] used for comparison as a point of reference. The VC-E criterion is defined as an upper level of 3.12 μm/s for the rms velocity amplitude spectrum at vibration frequencies <100 Hz. The criterion is very stringent and adequate for most of vibration-sensitive laboratory equipment. It is a common understanding that further improvement in vibration performance below the VC-E curve is impossible without great increase of cost of the lab design and construction.

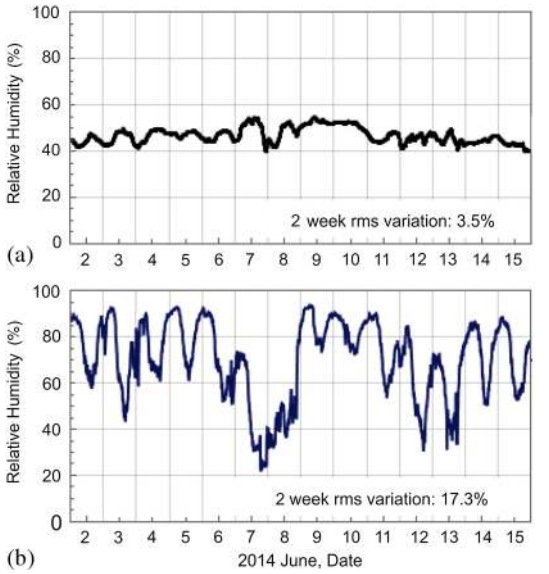

Fig. 5 (a) Variation of air relative humidity in the XROL cleanroom lab during 2 weeks in June 2014 and (b) variation of outside air relative humidity during the same 2 weeks.

3 X-Ray Optics Laboratory Metrology Instrumentation and Capabilities

The instrumental arrangement of the new ALS XROL is shown in Fig. 3. The instrumentation includes two slope measuring long-trace profilers, the LTP-II[34] and DLTP,[35] a 6-in. aperture interferometer, a ZYGO™ GPI,[40] two interferometric microscopes, a ZYGO™ NewView-7300[41,42] and a MicroMap™-570,[43] an atomic force microscope, a Veeco™ Dimension-3100,[44] an optical microscope, a NIKON™ MM-800/L, a differential laser Doppler vibrometer, a Polytec™ OFV-5000/OFV-552 (not shown in Fig. 3), and various systems for development and characterization of new x-ray optics, optics and mechanical systems, as well as for testing and calibration of the metrology instrumentation.[45–48] To fully realize the advantages of the XROL, a new, HZB/BESSY nano-optic measuring machine (NOM)-like,[49] high-precision granite gantry system with custom-built air-bearing translation systems capable of precision two-dimensional (2-D) scanning over the surface under test (SUT) and tilting and flipping the SUT has been purchased and recently installed in the lab. The system is a key element of the new instrument under development for surface slope metrology on the level of below 30 to 50 nrad. For the new lab, we have also purchased and installed a massive granite table for the LTP-II that is crucial for further improvement of the LTP-II's performance.

Usage of the broad spectrum of state-of-the-art metrology tools *ex situ* in the lab enables us to separately investigate and address different potential sources affecting beamline performance of an optic. These are surface quality (figure and finish errors), temporal and temperature dependence of surface shape, mechanical stability, gravity effects, alignments (twist, roll-off, yaw error), etc. At the beamline, all the perturbations produce a cumulative effect on the beamline performance of the optic that makes it difficult to optimize the optic's operational performance. The *ex situ* metrology allows us to fix the majority of the problems before installation of the optic at the beamline and to provide feedback on

design and guidelines for the best usage of the optic. Below, we briefly review the measurement capabilities and applications of main metrology instrumentation, available in the XROL.

3.1 *Updated LTP-II*

Recently after mounting the LTP-II[34] on the granite table, the instrument's detector was upgraded with a new CCD camera (PixeLINK 15.8MP GigE camera) with a significantly larger field of view. As a result of the upgrade, the LTP dynamic angular range in the tangential direction was extended from ~5 to 10 mrad.

The updated LTP-II provides one-dimensional surface slope profiling with the proven accuracy of tangential slope measurements with flat optics of <60 nrad rms and with significantly curved optics (radius of curvature of ≥15 m) of <250 nrad, limited by the instrumental systematic error. Normal orientation of the SUT is face up. With one or two additional pentaprisms, the LTP-II can be used to measure optics with side-facing and face-down orientations. These arrangements are usually used for setting and characterization of bendable mirrors and mirror assemblies designed for usage with a certain surface orientation. With additional pentaprisms, limitations due to the quality of the pentaprisms, their nonoptimal orientation and misalignment, lead to a significantly increased contribution of systematic error to the measurements. Note that the limitations are not so important when the task is to optimally shape a bendable mirror. This is because the slope trace measured along the entire clear aperture is used to optimize, via regression analysis, only two adjustment parameters that are the bender couplings.[50–52] Possessing a 2-D detector,[47] the upgraded LTP-II, when measuring tangential slope variation, also records the sagittal slope variation, allowing the characterization and repair of the mirror's twist and roll errors. Currently, the LTP-II dynamic slope range in the sagittal direction is ~15 mrad. The spatial resolution of the instrument is limited by the laser beam size of ~2.5 mm(tangential) × 4.0 mm(sagittal). The LTP-II is equipped with a lift that allows manually raising the instrument gantry system with the sensor carriage to accommodate for face-up measurements of an optical assembly with the total height of up to 27 in.

3.2 *Developmental LTP*

The developmental LTP[35] is a cost-efficient surface slope profilometer, based on an electronic AC ELCOMAT-3000 (as the one used in the BESSY-II NOM) and a movable mirror-based pentaprism.[53,54] The DLTP's dynamic slope range (in both, the tangential and the sagittal directions) is ±4.6 mrad; and the maximum tangential trace that can be measured is about 1 m. The range of applications of the DLTP is basically the same as the LTP-II. However, because of better spatial resolution (~1.7 mm with an aperture of 2.5 mm diameter[55–57]), accuracy, and temporal stability, the DLTP is the XROL's main tool for high accuracy metrology of x-ray optical substrates. The demonstrated accuracy of the measurements is of <50 nrad rms with flat optics and <100 nrad with significantly curved optics.[58] The improvement of performance of the upgraded DLTP in the XROL is discussed in Sec. 4.

3.3 *ZYGO™ GPI Fizeau Interferometer*

The 20-year old 6-in. ZYGO™ GPI Fizeau interferometer available at the XROL has rather limited accuracy due to imperfections of the reference flat and out-of-date design of the instrument. It is also very sensitive to air convection (turbulence) along the optical path. In the XROL due to the careful design of air recirculation, we are able to perform high repeatability interferometric tests with x-ray optics, enabling high accuracy differential measurements. This is used, for example, for precise and fast inspection of diffraction gratings, for alignment of optical assemblies, including parallelism and orthogonality of reflective optics, e.g., pairs of Kirkpatrick-Baez mirrors, and preliminary shaping of bendable optics. Unfortunately, the instrument's operation and control system, as well as the software, are obsolete and not upgradeable. Replacement by a modern instrument will significantly improve metrology at the spatial frequencies between the bandwidths of the LTP and the interferometric microscope and ensure 2-D surface metrology in the height domain at subnanometer levels of accuracy.

Availability in the optics lab of two different high performance, large field-of-view interferometers would allow cross-checking of measurements that is critical for understanding and suppression of the unavoidable systematic errors of the instruments, such as the systematic errors due to the limited quality of the reference optics built into the interferometers.

3.4 *ZYGO™ NewView-7300 and MicroMap™-570 Interferometric Microscopes*

The interferometric optical microscopes available at the XROL are the basic metrology tools for highly accurate testing of the surface finish of x-ray optics with subangstrom rms roughness measured over the mid-spatial wavelength region from ~1 μm to ~5 mm, corresponding to the frequency range of 0.2 to 10^3 mm^{-1}. The current flexible design of our MicroMap™-570 that is mounted on a long translational stage, with about 1-m travel, is very useful when surface roughness measurements with large optical assemblies are desired. In spite of its advanced age, the instrument still has very good optics and is capable of 0.5-A height resolution with minimal aberrations. In order to increase the application range and imply an original method for calibration of the instrumental modulation transfer function (MTF) (see Ref. 40 and references therein), we have developed a procedure and dedicated software for power spectral density (PSD) analysis of MicroMap™ measurements.[59] The PSD analysis enables measurements of groove density distributions of diffraction gratings as suggested and first realized in Ref. 43. The method consists of determination of the spatial frequency of the first harmonic peak appearing in the PSD distribution of the grating surface profile observed with a microscope. Using the MicroMap™-570 interferometric microscope, it was experimentally proven that this technique is capable of high-precision measurements with x-ray gratings with groove densities of about 250 grooves/mm, varying along the grating by 10%.

Besides the Micromap™-570 interferometric microscope, we have a new interferometric microscope, ZYGO™ NewView-7300. The distinguished features of the instrument are the capabilities for automatic repeatable

measurements with translation of the optic under test and measurements with stitching. This was used for groove density distribution measurements with a number variable-line-spacing gratings.[42] The demonstrated accuracy of measurements of groove density is about 0.10 grooves/mm for a 300-grooves/mm grating.

3.5 *Veeco™ Dimension-3100 Scanning Probe Microscope*

The scanning probe (atomic force) microscope (SPM) Veeco™ Dimension-3100 is the main instrumental modality at the XROL for imaging at the nanoscale at high spatial frequencies, 10 to 10^5 mm^{-1}, corresponding to the spatial wavelength range from ~100 μm to ~10 nm. One of the major applications of our SPM is for the research and development project on high-performance x-ray diffraction gratings (see, for example, Ref. 44 and references therein), providing information about shape and nanoroughness of the grating grooves. However, while the images of surfaces under test appear visually to be of a very high quality, from a metrological point of view, the reliability of measured images significantly suffers from limitations of the instrumental performance related to the uncertainty of resolution, instrumental aberrations, drift and noise, as well as detrending and contrast enhancement algorithms used to preprocess the images. The problem can be addressed via application of MTF calibration similar to one realized for other types of metrology instrumentation.[40]

4 Improvement of Performance of the Developmental Long Trace Profiler

After moving into the new lab, the DLTP was upgraded to optimize the measurements with side facing optics.[58] Figure 6 shows the experimental arrangement of the upgraded DLTP in the XROL.

4.1 *Temperature Variation Over the Developmental Long Trace Profiler Set-Up*

Figure 7 presents the results of measurement of temperature variation over the DLTP set-up. The locations of the temperature sensors used for characterization of the temperature stability of the DLTP set-up are marked with yellow squares in Fig. 6. In the course of the measurements in order to mimic normal operational conditions, the DLTP was running measurements over a 200-mm-long optical clear aperture.

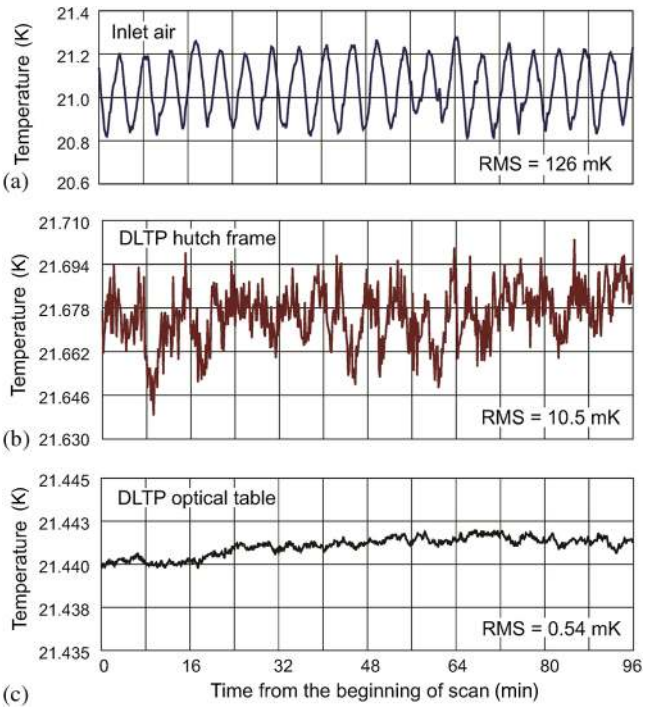

Fig. 7 The variation of the temperature of the inlet air is larger than the variation measured with the temperature sensors placed on the walls and used in the feedback loop of temperature stabilization. The difference between the mean values of the measured temperatures is mostly due to lack of calibration of the temperature sensors. (a) Inlet air; (b) DLTP hutch frame; and (c) DLTP optical table.

The inlet air temperature (Fig. 7), recorded with a sensor located right below the fabric duct, has a periodic oscillation with amplitude of about ±200 mK and period of ~5 min. The variation of the temperature of the inlet air is larger than the variation measured with the temperature sensors placed on the walls and used in the feedback loop of temperature stabilization. The amplitude of the oscillation is significantly reduced to about ±25 mK, when temperature is measured on the DLTP hutch frame. The amplitude of temperature variation measured on the top of the DLTP optical table is extremely small, approximately ±1.4 mK rms. This temperature variation does not noticeably affect the slope

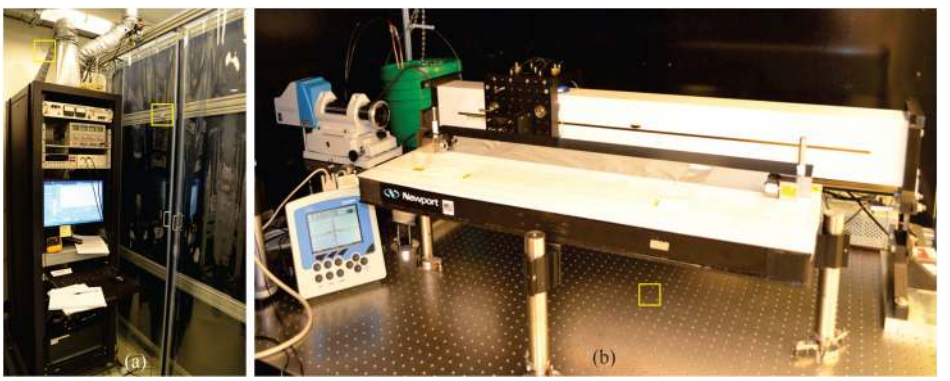

Fig. 6 Arrangement of the upgraded DLTP: (a) hutch and the DAC system rack and (b) DLTP experimental set-up with an 880-mm long flat super polished substrate of M301 mirror for the ALS BL 8.3.1. The locations of the temperature sensors used for characterization of the temperature stability of the DLTP set-up are marked with the yellow squares.

metrology with side facing optics (see also the data in Fig. 11 and the corresponding discussion in Sec. 4.3).

4.2 *Air-Bearing Pressure Variation*

In the course of recommissioning in the new lab, we investigated the temporal stability of the DLTP set up with a set of two tiltmeters, arranged in the differential mode to measure the pitch angle variation of the unmoved DLTP carriage with activated air bearings.[46] In order to monitor the pitch angle variation with the AC, a reference mirror was mounted to the carriage in front of the AC. The AC vertical angular signal is recorded. Additionally, two tiltmeters, one placed on the DLTP carriage and the other one on the DLTP optical table, are used in the differential mode to monitor the carriage wobbling.

The results of the DLTP stability test are presented in Fig. 8. The strong correlation between the tiltmeter and the AC measurements and significant difference of the variation from the temperature oscillation in Fig. 7 suggest that the origin of the pitch angle variation is due to the variation of the air pressure supplied to the carriage air bearings. There is such a variation of the yaw angle. The variation of the roll angle is much smaller. A similar pitch angular variation was observed with the SPring-8 long trace profiler.[60]

A known way to reduce the air-bearing pressure variation is to use a large volume reservoir tank in line with the high-pressure airline supplying the air bearings and to optimize the flow rate of air coming to the tank with an input valve. In our case, additional optimization is possible due to the relatively large volume (estimated to be $V_P \approx 20-30$ liters) of the pipes connecting the reservoir tank ($V_T \approx 200$ liters) with the DLTP and LTP-II carriages (see Appendix A).

Figure 9 shows a simplified schematic of the pressured airline, supplying the DLTP and LTP-II air-bearing systems used for the DLTP air-bearing pressure measurement and optimization.

As analytically derived in Appendix A, with the practical limit $(\lambda_{\mathrm{IN}} + \lambda_P + \lambda_{\mathrm{OUT}}) \ll \Omega$, where λ_{IN} and λ_P are the filling rates of the tank and the pipe volume, respectively, λ_{OUT} is the tank deflation rate, and Ω is the frequency of the input pressure oscillation, the amplitude of the output pressure oscillation is suppressed by a factor of

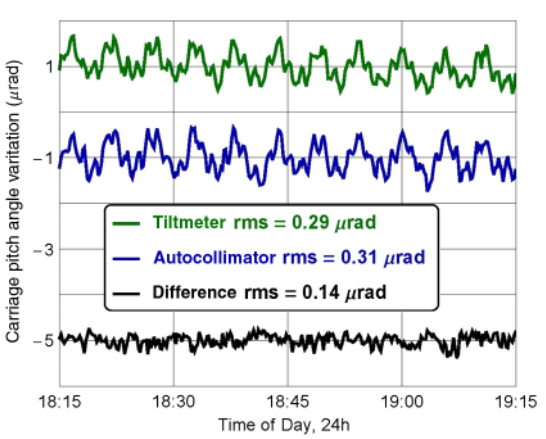

Fig. 8 Stability test of pitch angle of the DLTP carriage: the pitch variation as a differential signal of the two tiltmeters (the top green trace), the AC vertical angular signal (the medium blue trace), and the difference of the tiltmeter and the AC measurements (the bottom black trace).

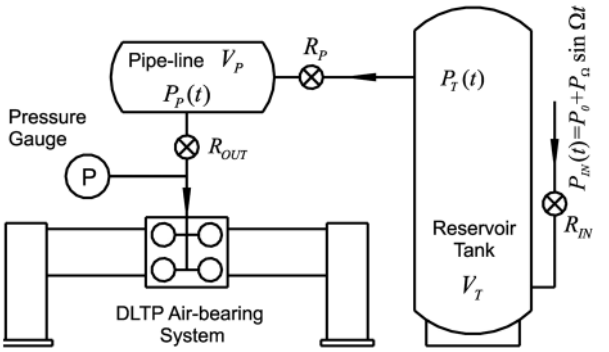

Fig. 9 Simplified schematic of the pressured air-line, supplying the DLTP and LTP-II air-bearing systems. The notations in the schematic are used and explained in Appendix A.

$$\gamma \approx \frac{\lambda_{\mathrm{IN}}}{\Omega} \cdot \frac{\lambda_P}{\Omega}, \tag{1}$$

which has an additional suppression factor λ_P/Ω, compared to the suppression in the case of a single reservoir tank. Practically, the optimization consists of adjustment of the parameters λ_{IN} and λ_P to the lowest possible level, at which the output air pressure is still high enough for normal operation of the carriage air-bearing system.

The result of the optimization is presented in Fig. 10. A reduction of the supplied pressure ~14% suppresses the air-bearing pressure variation by a factor of ~200.

Stability tests, performed with the upgraded DLTP after all optimizations of the instrumental performance discussed above were completed, have demonstrated an almost random variation of the AC readings with an rms variation in a single trace of 80 and 150 nrad (including a drift) in the horizontal (optimized tangential) and the vertical (sagittal) AC channels, respectively. These correspond to the effective measurement instability upon averaging eight traces, recorded according to the scanning strategy, optimal for effective suppression of the instrumental drift described with the third degree polynomial,[61] of 27 nrad (rms) and 35 nrad (rms) in the horizontal and the vertical AC channels, respectively.

4.3 *Developmental Long Trace Profiler Performance in Measurements with a Long Plane Mirror Substrate*

An example of an effect of improvement of the lab environmental conditions on the *ex situ* metrology is the recent characterization of an 880 long super-polished plane substrate, carried out in the XROL with the upgraded DLTP (Fig. 6). The internally cooled single crystal silicon substrate was fabricated for the M301 elliptically bent mirror for the ALS macromolecular crystallography superbend beamline 8.3.1.[62] The specified clear aperture of the mirror is 750 mm. The results of the measurements are summarized in Fig. 11.

Each measurement in Fig. 11 is a result of averaging over eight scans with 1-mm increment performed according to an optimal scanning strategy.[61] The data in the left-hand column presents a stability test. In this case, two sequential measurements were made without any adjustment or realignment of the experimental set-up between the measurements. Half of the difference can be used as a measure of the measurement repeatability (with respect to the averaged trace). The

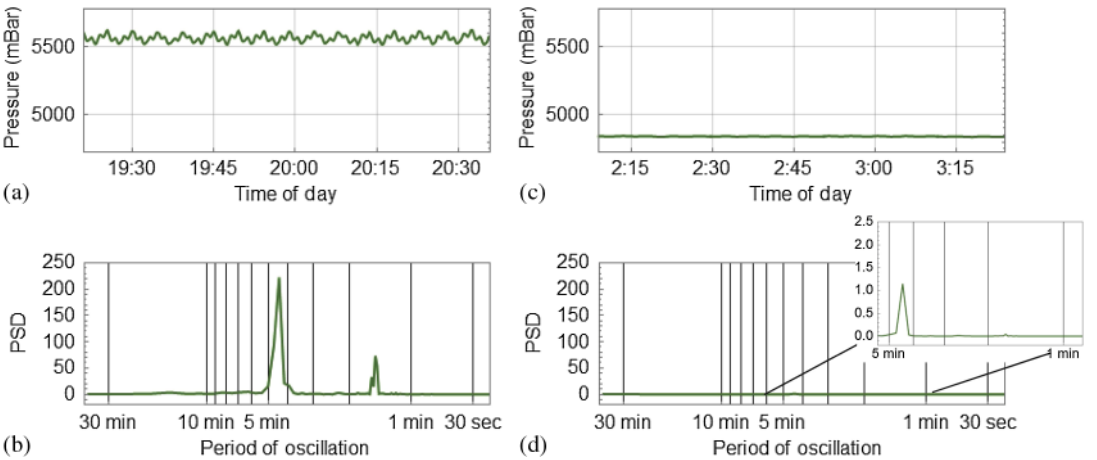

Fig. 10 (a) The DLTP air-bearing pressure variation measured with the input valve totally opened; (b) the power spectral density (PSD) of the pressure variation in plot (a); (c) the variation of the air-bearing pressure with the input valve optimally opened; (d) the PSD of the pressure variation in plot (c). The major PSD peak at the period of oscillation of about 4.5 min, enlarged in the inset of plot (d), has the amplitude by a factor of ~200 smaller than the corresponding peak in plot (b). Note that there two main harmonics of pressure oscillation in the house pressured airline.

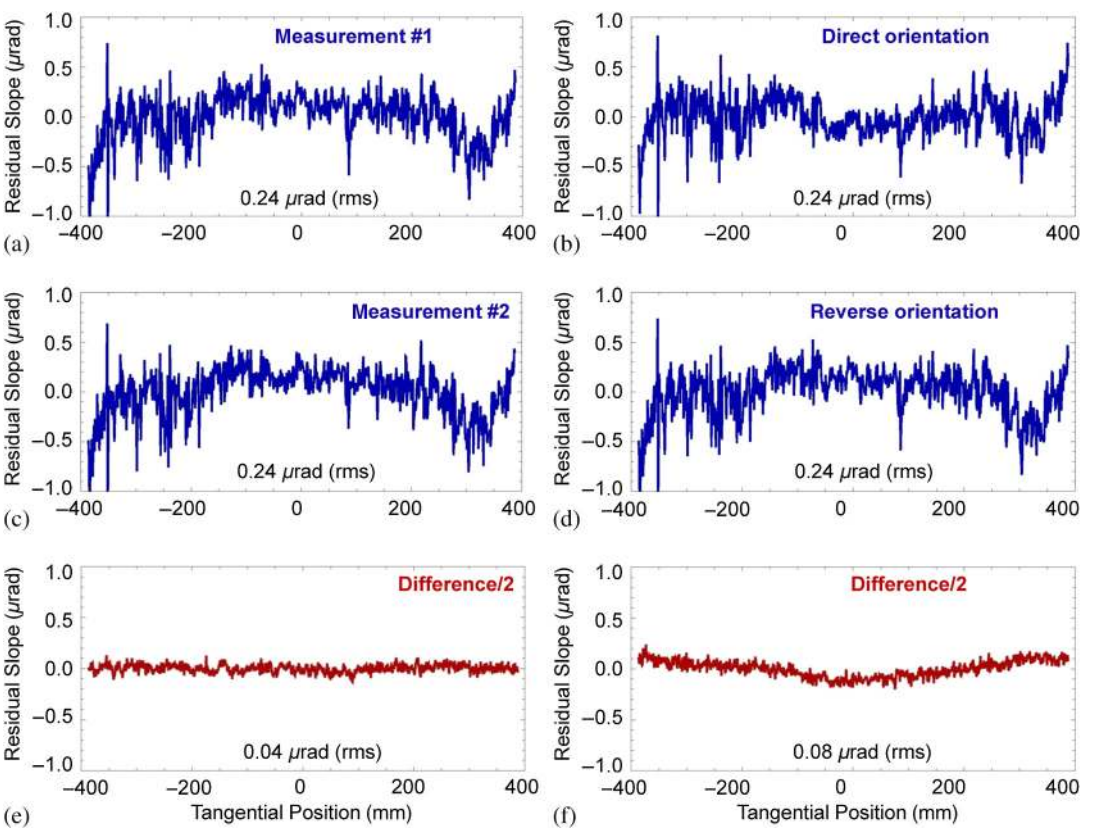

Fig. 11 The results of the DLTP measurements with the 880-mm long plane mirror substrate of M301 mirror for the ALS BL8.3.1. Each measurement is a result of averaging over eight scans with 1-mm increment performed according to the optimal scanning strategy.[61] The duration of one measurement is about 8 h. Two pairs of sequential measurements used for the DLTP stability test, plots (a) and (c), and for evaluation of the residual systematic error, plots (b) and (d). (e) and (f) The corresponding traces of half of the difference of the measurements.

residual systematic error can be estimated from the data in the right-hand column in Fig. 11. Here, two sequential measurements with the different, direct and reversed (flipped), orientations of the substrate are considered. The resulting half of the difference of the measurements of about 80 nrad (rms) can be thought of as a measure of the instrumental systematic error in a single measurement with flat optics (also with respect to the averaged trace). Note that the measured systematic error is partially due to the misalignment of the traces under comparison after flipping the optic.

Therefore, the current arrangement of the DLTP in the new optics lab yields measurements in under 8 h with the rms error

<80 nrad (including the instrumental random, systematic, and drift errors) for a long, 750-mm clear aperture, flat optic. The measurement accuracy is limited in most part by the trace positioning and performance of the DLTP AC that was not calibrated for this specific arrangement. This should be compared with more than a week-long measurement required for an equivalent metrology in the old lab.

5 Conclusions

We have discussed the main concepts and approaches essential for construction and successful operation of a modern metrology facility for x-ray optics. First of all, the dedicated laboratory must provide extremely stable environmental conditions, adequate to the ultimate performance of state-of-the-art metrology instruments in the lab. We have described the key specification parameters that, with careful attention to, allowed us to build a lab with temperature stability, air cleanness, air convection and turbulence, and humidity variation significantly better than can be directly specified with reasonably small construction funding. For example, in the new lab we achieve better particulate control than officially specified by a factor of more than 20 and better temperature stability by a factor of 4.

We have investigated the effect on the DLTP performance of 4.5-min oscillations of air pressure, supplied to the instrument's air-bearing system. We have analytically shown that the usage of two in-serial damping reservoirs allows significant suppression of the variation. In this case, the suppression factor is approximately a product of that of each reservoir. After corresponding optimization, this method has allowed us to suppress the DLTP air-bearing pressure variation by a factor of ~200 at a reduction of the supplied pressure by only ~14%.

As an example of the improvement of metrology efficiency due to the advanced environmental conditions in the new lab, we have presented the results of surface slope metrology of an internally cooled single crystal silicon flat substrate performed with the upgraded DLTP, available now at the XROL. We have demonstrated that the current arrangement of the DLTP, optimized for side facing optics, yields measurements in under 8 h with the rms error <80 nrad (including the instrumental random, systematic, and drift errors) for a long, 750-mm clear aperture, flat optic. The error is limited in most part by the finite accuracy of trace positioning and inherent performance (systematic error) of the DLTP AC. The measurement repeatability has shown to be on the level of 40 nrad (rms), adequate to successful application of rigorous calibration methods to suppress the systematic error. For comparison, to obtain equivalent metrology as that of a single 8-h run of the DLTP in the new XROL, it would have taken more than a week long measurement in the old lab.

The advanced environmental conditions in the new lab provide the foundation for research and development on high accuracy instrumentation that is an inseparable part of the ALS program on radical improvement of on-site x-ray optical metrology.

To meet the challenge of measuring mirrors, including strongly curved ones, with slope errors at the level <50 nrad, the absolute accuracy of a new slope profilometer must be better at least by a factor of 2 to 3.[63,64] The key point for improvement is reduction of the instability and systematic error, inherent to the instrument. We address these problems in a new profiler under development. The profiler is based on a NOM-like granite gantry system, capable of precision 2-D slope metrology.[65,66] An automatic rotation, flipping, and alignment stage is designed to implement effective suppression of measurement errors via fully automatic measurements according to the developed optimal scanning strategies.[22,45,61] One of the prospective sensors for the profiler is an LTP-type multibeam optical sensor that is under development in collaboration with the metrology team at NASA Marshall Space Flight Center (see Ref. 67 and references therein). Recently, a 2-D slope measuring system based on stitching measurements with a Shack–Hartmann optical head was reported to be capable of providing high-accuracy automated metrology for x-ray mirrors with slope error accuracy better than 50 nrad (rms).[68] This approach is also under consideration and the corresponding cross check measurements are in progress.

To support the program on the development of high-resolution x-ray diffraction gratings, we need tools that allow high accuracy evaluation of line density distributions. Recent investigations, performed at the XROL, have established the scope of such a research and development program based on combining the measurements performed with a slope measuring profiler and with an interferometric microscope.[42,69–73]

Development of high-performance calibration methods and tools is vital for improving measurement accuracy. In collaboration with HZB/BESSY-II and PTB (Germany) metrology teams, we are working on an original method for angular calibration of surface slope profilometers. The method is based on a concept of a universal test mirror (UTM).[74] Recently, a keystone of the UTM system, a custom high-precision tilting stage, has been purchased and tested.[75] The tests were based on a comparison of calibrations of the AC, obtained with the UTM tilting stage, with the calibration, performed at the PTB using the high-precision angular comparator.[29,30] The tests have demonstrated agreement of the calibrations on the level better than 30 nrad (rms).[75] The work on development of a full-scale UTM system is in progress.

In summary, the next generation of mirror measurement tools must target sensitivity and accuracy values well below the actual current level and will need to meet the optimal quality of the new x-ray sources (diffraction limited). It has become apparent that without the development of effective, broadly applicable *ex situ* and *in situ* metrology techniques, costly increases in source brightness may hardly be noticed in end-station sample chambers. There are literally orders of magnitude in metrology performance to be gained by the development of new measurement techniques, instrumentation and procedures, to satisfy the ever-increasing demand for greater accuracy, increased reliability, and rapidity of measurements with super high-quality x-ray optics.[14]

Appendix A: Analytical Solution for Suppression of Air Pressure Variation in the DLTP Air-Bearing Systems

Here, we briefly outline the analytical foundation of the method of suppression of air pressure variation in the DLTP and LTP-II air-bearing systems, discussed in Sec. 4.2. A schematic of the pressured airline under consideration,

with a reservoir tank and a relatively large-volume pipeline, is shown in Fig. 9.

A1 Variation of Pressure in a System with a Single Reservoir Tank

Let us assume that the input pressure P_{IN} of the building pressured airline (Fig. 9) has a harmonic variation with respect to the average pressure P_0 with a frequency Ω and an amplitude P_Ω:

$$P_{\mathrm{IN}}(t) = P_0 + P_\Omega \sin \Omega t. \tag{2}$$

As a good approximation in our case, the flow into the reservoir tank is proportional to the difference between the input pressure $P_{\mathrm{IN}}(t)$ and the pressure inside the tank $P_T(t)$. The coefficient of proportionality λ_{IN} that is the tank-filling rate is

$$\lambda_{\mathrm{IN}} = R_{\mathrm{IN}}/V_T, \tag{3}$$

where R_{IN} is the flow rate through the valve in the units of volume/unit time and V_T is the volume of the tank. Parameter R_{IN} is controlled with the input valve (Fig. 9) and is the subject of optimization. In this notation, a differential equation for the tank pressure is

$$\frac{dP_T(t)}{dt} = -\lambda_{\mathrm{IN}}[P_T(t) - P_{\mathrm{IN}}(t)] - \lambda_{\mathrm{OUT}}[P_T(t) - P_A]. \tag{4}$$

In Eq. (4), $\lambda_{\mathrm{OUT}} = R_{\mathrm{OUT}}/V_T$ is the tank deflation rate, where R_{OUT} is the flow rate through the air-bearings in the units of volume/unit time, and P_A is the atmospheric pressure.

A stationary (in the limit of very large t, $t \to \infty$) solution of Eq. (4) is

$$P_T(t) = \frac{\lambda_{\mathrm{IN}}P_0 + \lambda_{\mathrm{OUT}}P_A}{\lambda_{\mathrm{IN}} + \lambda_{\mathrm{OUT}}} + P_\Omega \frac{\lambda_{\mathrm{IN}}}{\sqrt{\Omega^2 + (\lambda_{\mathrm{IN}} + \lambda_{\mathrm{OUT}})^2}} \sin(\Omega t - \theta), \tag{5}$$

where the phase shift θ is given by

$$\sin\theta \equiv \frac{\Omega}{\sqrt{\Omega^2 + (\lambda_{\mathrm{IN}} + \lambda_{\mathrm{OUT}})^2}} \quad \text{or, equivalently,} \quad \cos\theta \equiv \frac{\lambda_{\mathrm{IN}} + \lambda_{\mathrm{OUT}}}{\sqrt{\Omega^2 + (\lambda_{\mathrm{IN}} + \lambda_{\mathrm{OUT}})^2}}. \tag{6}$$

The corresponding relative suppression of the pressure variation, defined as a ratio of the oscillation amplitude in Eq. (5), to the corresponding average pressure is

$$\zeta = \frac{(\lambda_{\mathrm{IN}} + \lambda_{\mathrm{OUT}})}{\sqrt{\Omega^2 + (\lambda_{\mathrm{IN}} + \lambda_{\mathrm{OUT}})^2}} \left(\frac{P_0}{P_0 + P_A(\lambda_{\mathrm{OUT}}/\lambda_{\mathrm{IN}})}\right). \tag{7}$$

With practical limits: $\lambda_{\mathrm{IN}}P_0 \gg \lambda_{\mathrm{OUT}}P_A$ and $(\lambda_{\mathrm{IN}} + \lambda_{\mathrm{OUT}}) \ll \Omega$, we have

$$\zeta \approx \frac{(\lambda_{\mathrm{IN}} + \lambda_{\mathrm{OUT}})}{\Omega} \ll 1. \tag{8}$$

For efficient suppression of the input pressure variation, the total flow rates through the tank input and output valves, $(R_{\mathrm{IN}} + R_{\mathrm{OUT}})$, should be as small as possible and the tank volume, V_T, as large as possible, in order to provide $\Omega \gg (\lambda_{\mathrm{IN}} + \lambda_{\mathrm{OUT}})$.

A2 Variation of Pressure in a System with Two Large Reservoirs

In order to account for an additional reservoir volume of the pipes with a time-dependent pressure $P_P(t)$, we replace the atmospheric pressure with the pressure inside the pipe volume in Eq. (4), and we write an additional equation analogous [Eq. (4)] for the pressure inside the pipe:

$$\frac{dP_T(t)}{dt} = -(\lambda_{\mathrm{IN}} + \lambda_P)P_T(t) + \lambda_{\mathrm{IN}}P_0 + \lambda_{\mathrm{IN}}P_\Omega \sin \Omega t + \lambda_P P_P(t), \tag{9}$$

$$\frac{dP_P(t)}{dt} = -(\lambda_P + \lambda_{\mathrm{OUT}})P_P(t) + [\lambda_P P_T(t) + \lambda_{\mathrm{OUT}}P_A], \tag{10}$$

where λ_P is the pipe volume filling rate:

$$\lambda_P = R_P/V_P, \tag{11}$$

where R_P is the flow rate from the reservoir tank to the pipe volume, defined in the units of volume/unit time. Parameter R_P is the subject of optimization by adjusting the second (output) valve attached to the tank [Fig. 9(c)]. Note that in Eq. (10), $\lambda_{\mathrm{OUT}} = R_{\mathrm{OUT}}/V_P$.

A stationary ($t \to \infty$) solution of the system of first-order differential equations [Eq. (9)] is

$$P_P(t) = \frac{\lambda_{\mathrm{EFF}}^2 P_{\mathrm{EFF}}}{b} + P_\Omega \frac{c}{\sqrt{a^2\Omega^2 + (\Omega^2 - b)^2}} \sin(\Omega t - \theta) \tag{12}$$

with the parameters:

$$a = 2\lambda_P + \lambda_{\mathrm{IN}} + \lambda_{\mathrm{OUT}},$$
$$b = \lambda_P\lambda_{\mathrm{IN}} + \lambda_{\mathrm{OUT}}\lambda_{\mathrm{IN}} + \lambda_P\lambda_{\mathrm{OUT}},$$
$$c = \lambda_P\lambda_{\mathrm{IN}},$$
$$\lambda_{\mathrm{EFF}}^2 P_{\mathrm{EFF}} = (\lambda_{\mathrm{IN}} + \lambda_P)\lambda_{\mathrm{OUT}}P_A + \lambda_P\lambda_{\mathrm{IN}}P_0. \tag{13}$$

The phase shift θ in Eq. (12) is given by

$$\sin\theta \equiv \frac{a\Omega}{\sqrt{a^2\Omega^2 + (\Omega^2 - b)^2}} \quad \text{or, equivalently,} \quad \cos\theta \equiv \frac{\Omega^2 - b}{\sqrt{a^2\Omega^2 + (\Omega^2 - b)^2}}. \tag{14}$$

With the practical limit $(\lambda_{\mathrm{IN}} + \lambda_P + \lambda_{\mathrm{OUT}}) \ll \Omega$, we have the amplitude of the pressure variation suppressed by a factor of

$$\gamma \approx \frac{\lambda_{\mathrm{IN}}}{\Omega} \cdot \frac{\lambda_P}{\Omega}, \tag{15}$$

which has an additional suppression factor λ_P/Ω, compared to the suppression in the case of a single reservoir tank [compare with condition Eq. (8)].

It is easy to check by straightforward substitution of parameters [Eq. (13)] into solution [Eq. (12)] that there is an additional additive term in the reduction of the average pressure, described with the ratio $\lambda_{\mathrm{OUT}}/\lambda_P$. However, in our case, when $V_P \ll V_T$, this additional pressure reduction is relatively small.

Acknowledgments

The authors are very grateful to Erik Anderson, Lahsen Assoufid, Sergey Babin, Samuel Barber, Nathalie Bouet, Richard Celestre, Elaine Chan, Weilun Chao, Arthur Chaubard, Kenneth Chow, Raymond Conley, Curtis Cummings, Edward Domning, Roger Falcone, Ralf Geckeler, Kenneth Goldberg, Tennessee Gock, Mikhail Gubarev, Eric Gullikson, Mourad Idir, Konstantine Kaznatcheev, Nicholas Kelez, Jonathan Kirschman, Igor Kozhevnikov, James Macdougall, Elizabeth Martin, Daniel Merthe, Iacopo Mochi, Gregory Morrison, Simon Morton, Patrick Naulleau, Tino Noll, Steve Rossi, Liubov Samoylova, Ross Schaefer, Frank Siewert, Brian Smith, Regina Soufli, Charles Taberski, Peter Takacs, Jeffrey Takakuwa, Monroe Thomas, Jeff Troutman, Anastasia Tyurina, Yuri Tyurin, Tony Warwick, Christopher Weyandt, Erin Wood, Yekaterina Yashchuk, Anthony Young, Brett Young, Sam Yuan, and Thomas Zeschke for extremely productive and enjoyable collaboration on development and application of metrology for x-ray optics at the ALS. The Advanced Light Source is supported by the Director, Office of Science, Office of Basic Energy Sciences, Material Science Division, of the U.S. Department of Energy under Contract No. DE-AC02-05CH11231 at Lawrence Berkeley National Laboratory. This work was supported in part by the UC Office of the President, Proof of Concept Grant ID No. 268826 and by the U.S. Department of Energy Office of Science, Office of Basic Energy Sciences Energy Small Business Technology Transfer (STTR) program under Award No. DE-SC0011352.

References

1. M. Eriksson and J. F. van der Veen, "Special issue on diffraction-limited storage rings and new science opportunities," *J. Synchrotron Radiat.* **21**(5), 837–1216 (2014).
2. R. Hettel and M. Borland, "Perspectives and challenges for diffraction limited storage ring light sources," in *Proc. of PAC2013, MOYAB1*, Pasadena, California, pp. 19–23 (2013).
3. "Grand challenge science on diffraction-limited storage rings," A consensus report on future opportunities from scientists at ALS, LBNL; APS, ANL; NSLS-II, BNL; SSRL, SLAC together with a broad community of scientists at laboratories and universities, BESAC Subcommittee on Future Light Sources, http://www.aps.anl.gov/Upgrade/Documents/DLSR_report_for_BESAC.pdf (2013).
4. The advanced light source strategic plan 2014-18, http://www-als.lbl.gov/images/stories/News_and_Publications/General_Publications/strategic_plan_2014-18.pdf (10 February 2015).
5. R. Barrett, "Precision and stability issues for x-ray optics systems," in *Presentation at the 4th DLSR Workshop*, APS, Argonne (2014).
6. D. Cocco, "Recent developments in UV optics for ultra-short, ultra-intense coherent light sources," *Photonics* **2**(1), 40–49 (2015).
7. A. Marechal, "Etude des effects combines de la diffraction et des aberrations geometriques sur l'image d'un point lumineux," *Revue d'Optique* **26**, 257–277 (1947).
8. M. Born and E. Wolf, *Principles of Optics*, 7th ed., Sec. IX, Cambridge University Press (1999).
9. E. L. Church and P. Z. Takacs, "Specification of surface figure and finish in terms of system performance," *Appl. Opt.* **32**(19), 3344–3353 (1993).
10. E. L. Church and P. Z. Takacs, "Specification of glancing- and normal-incidence x-ray mirrors," *Opt. Eng.* **34**(2), 353–360 (1995).
11. L. Samoylova et al., "Requirements on hard x-ray grazing incidence optics for European XFEL: analysis and simulation of wavefront transformations," *Proc. SPIE* **7360**, 73600E (2009).
12. V. V. Yashchuk, L. Samoylova, and I. V. Kozhevnikov, "Specification of x-ray mirrors in terms of system performance: a new twist to an old plot," *Proc. SPIE* **9209**, 92090F (2014).
13. V. V. Yashchuk, L. Samoylova, and I. V. Kozhevnikov, "Specification of x-ray mirrors in terms of system performance: a new twist to an old plot," *Opt. Eng.* **54**(2), 025108 (2015).
14. M. Idir and V. V. Yashchuk, "Optical and x-ray metrology," in *X-ray Optics for BES Light Source Facilities, Report of the Basic Energy Sciences Workshop on X-ray Optics for BES Light Source Facilities*, D. Mills and H. Padmore, Eds., pp. 44–55, U.S. Department of Energy, Office of Science, Potomac, Maryland (2013).
15. V. V. Yashchuk, "Advanced x-ray optics metrology," *Synchrotron Radiat. News* **26**(5), 2–3 (2013).
16. F. Siewert et al., "On the characterization of ultra-precise x-ray optical components: advances and challenges in ex situ metrology," *J. Synchrotron Radiat.* **21**, 968–975 (2014).
17. P. Z. Takacs, "X-ray optics metrology," Chapter 46 in *Handbook of Optics*, 3rd ed., V. M. Bass, Ed., McGraw-Hill, New York (2009).
18. K. Yamauchi et al., "Figuring with sub-nanometer-level accuracy by numerically controlled elastic emission machining," *Rev. Sci. Instrum.* **73**(11), 4028–4033 (2002).
19. K. Yamauchi et al., "Microstitching interferometry for x-ray reflective optics," *Rev. Sci. Instrum.* **74**(5), 2894–2898 (2003).
20. H. Mimura et al., "Relative angle determinable stitching interferometry for hard x-ray reflective optics," *Rev. Sci. Instrum.* **76**(4), 045102 (2005).
21. K. Yamauchi et al., "Single-nanometer focusing of hard x-rays by Kirkpatrick-Baez mirrors," *J. Phys. Condens. Matter* **23**, 394206 (2011).
22. V. V. Yashchuk et al., "Correlation analysis of surface slope metrology measurements of high quality x-ray optics," *Proc. SPIE* **8848**, 88480I (2013).
23. F. Polack et al., "An LTP stitching procedure with compensation of instrument errors: Comparison of SOLEIL and ESRF results on strongly curved mirrors," *Nucl. Instrum. Methods A* **616**(2–3), 207–211 (2010).
24. H. Yumoto et al., "Stitching-angle measurable microscopic-interferometer: surface-figure metrology tool for hard x-ray nanofocusing mirrors with large curvature," *Nucl. Instrum. Methods A* **616**(2–3), 203–206 (2010).
25. F. Siewert, J. Buchheim, and T. Zeschke, "Characterization and calibration of 2nd generation slope measuring profiler," *Nucl. Instrum. Methods A* **616**(2–3), 119–127 (2010).
26. M. Schulz, G. Ehret, and P. Křen, "High accuracy flatness metrology within the European Metrology Research Program," *Nucl. Instrum. Methods A* **710**, 37–41 (2013).
27. V. V. Yashchuk et al., "Air convection noise of pencil-beam interferometer for long-trace profiler," *Proc. SPIE* **6317**, 63170D (2006).
28. PTB Info Sheet, *The Clean Room Center of PTB*, Physikalisch-Technische Bundesanstalt, Press and Information Office, Braunschweig (2015).
29. R. Probst et al., "The new PTB angle comparator," *Meas. Sci. Technol.* **9**, 1059–1066 (1998).
30. R. D. Geckeler and A. Just, "Optimized use and calibration of autocollimators in deflectometry," *Proc. SPIE* **6704**, 670407 (2007).
31. P. E. Ciddor, "Refractive index of air: New equations for the visible and near infrared," *Appl. Opt.* **35**(9), 1566–1573 (1996).
32. National Institute of Standards and Technology's Web site, "Refractive index of air calculator," http://emtoolbox.nist.gov/Wavelength/Ciddor.asp (10 February 2015).
33. H. Yumoto et al., "Absolute calibration of optical flats using the three-flat test by considering the relative humidity change," *Nucl. Instrum. Methods A* **710**, 2–6 (2013).
34. J. L. Kirschman et al., "Performance of the upgraded LTP-II at the ALS Optical Metrology Laboratory," *Proc. SPIE* **7077**, 70770A (2008).
35. V. V. Yashchuk et al., "Sub-microradian surface slope metrology with the ALS developmental long trace profiler," *Nucl. Instrum. Methods A* **616**(2–3), 212–223 (2010).
36. "High performance cleanrooms: a design guidelines sourcebook," 2011, http://www.pge.com/includes/docs/pdfs/mybusiness/energysavingsrebates/incentivesbyindustry/Cleanrooms_BestPractices.pdf (10 February 2015).
37. TerraUniversal.com, "FS209E and ISO Cleanroom Standards," http://www.terrauniversal.com/cleanrooms/iso-classification-cleanroom-standards.php (10 February 2015).
38. C. G. Gordon, "Generic vibration criteria for vibration-sensitive equipment," *Proc. SPIE* **3786**, 22–33 (1999).

39. H. Amick et al., "Evolving criteria for research facilities: vibration," *Proc. SPIE* **5933**, 593303 (2005).
40. V. V. Yashchuk et al., "Calibration of the modulation transfer function of surface profilometers with binary pseudo-random test standards: expanding the application range to Fizeau interferometers and electron microscopes," *Opt. Eng.* **50**(9), 093604 (2011).
41. I. Lacey et al., "High precision surface metrology of x-ray optics with an interferometric microscope," *Proc. SPIE* **8838**, 883808 (2013).
42. V. V. Yashchuk, W. R. McKinney, and N. A. Artemiev, "Ex situ metrology of x-ray diffraction gratings," *Nucl. Instrum. Methods A* **710**, 59–66 (2013).
43. V. V. Yashchuk et al., "Two-dimensional power spectral density measurements of X-ray optics with the MicromapTM interferometric microscope," *Proc. SPIE* **5858**, 58580A (2005).
44. D. L. Voronov et al., "Control of surface mobility for conformal deposition of Mo-Si multilayers on saw-tooth substrates," *Appl. Surf. Sci.* **284**, 575–580 (2013).
45. Z. Ali et al., "Automated suppression of errors in LTP-II slope measurements with x-ray optics," *Proc. SPIE* **8141**, 81410O (2011).
46. J. L. Kirschman et al., "Precision tiltmeter as a reference for slope measuring instruments," *Proc. SPIE* **6704**, 670409 (2007).
47. J. L. Kirschman et al., "Flat-field calibration of CCD detector for long trace profilers," *Proc. SPIE* **6704**, 67040J (2007).
48. R. Geckeler et al., "Autocollimators for deflectometry: current status and future progress," *Nucl. Instrum. Methods A* **616**(2–3), 140–146 (2010).
49. F. Siewert, H. Lammert, and T. Zeschke, "The nanometer optical component measuring machine," in *Modern Developments in X-Ray and Neutron Optics*, A. Erko et al., Eds., Springer, New York (2008).
50. W. R. McKinney et al., "Optimal tuning and calibration of bendable mirrors with slope measuring profilers," *Opt. Eng.* **48**(8), 083601 (2009).
51. W. R. McKinney et al., "*Ex situ* tuning of bendable x-ray mirrors for optimal beamline performance," *Proc. SPIE* **8501**, 850109 (2012).
52. N. A. Artemiev et al., "Optimal setting of bendable optics based on FEA calculations," *Proc. SPIE* **8501**, 850107 (2012).
53. S. K. Barber et al., "Developmental long trace profiler using optimally aligned mirror based pentaprism," *Opt. Eng.* **50**(5), 053601 (2011).
54. S. K. Barber et al., "Optimal alignment of mirror based pentaprism for scanning deflectometric devices," *Opt. Eng.* **50**(7), 073602 (2011).
55. Y. V. Yashchuk and V. V. Yashchuk, "Reliable before-fabrication forecasting of expected surface slope distributions for x-ray optics," *Proc. SPIE* **8141**, 81410N (2011).
56. Y. V. Yashchuk and V. V. Yashchuk, "Reliable before-fabrication forecasting of expected surface slope distributions for x-ray optics," *Opt. Eng.* **51**(4), 046501 (2012).
57. F. Siewert et al., "Investigations on the spatial resolution of autocollimator-based slope measuring profilers," *Nucl. Instrum. Methods A* **710**, 42–47 (2013).
58. I. Lacey et al., "The developmental long trace profiler (DLTP) optimized for metrology of side-facing optics at the ALS," *Proc. SPIE* **9206**, 920603 (2014).
59. V. V. Yashchuk et al., "Surface roughness of stainless steel mirrors for focusing soft x-rays," *Appl. Opt.* **45**(20), 4833–4842 (2006).
60. Y. Senba et al., "Upgrade of long trace profiler for characterization of high-precision X-ray mirrors at SPring-8," *Nucl. Instrum. Methods A* **616**(2–3), 237–240 (2010).
61. V. V. Yashchuk, "Optimal measurement strategies for effective suppression of drift errors," *Rev. Sci. Instrum.* **80**, 115101 (2009).
62. A. A. MacDowell et al., "Suite of three protein crystallography beamlines with single superconducting bend magnet as the source," *J. Synchrotron Radiat.* **11**, 447–455 (2004).
63. V. V. Yashchuk et al., "Development of a new generation of optical slope measuring profiler," *Nucl. Instrum. Methods A* **649**(1), 153–155 (2011).
64. L. Assoufid et al., "Development of a high-performance gantry system for a new generation of optical slope measuring profilers," *Nucl. Instrum. Methods A* **710**, 31–36 (2013).
65. H. Thiess, H. Lasser, and F. Siewert, "Fabrication of X-ray mirrors for synchrotron applications," *Nucl. Instrum. Methods A* **616**(2–3), 157–161 (2010).
66. F. Siewert et al., "Ultra-precise characterization of LCLS hard x-ray focusing mirrors by high resolution slope measuring deflectometry," *Opt. Exp.* **20**(4), 4525–4536 (2012).
67. M. V. Gubarev et al., "Status of multi-beam long trace-profiler development," *Proc. SPIE* **8848**, 88480L (2013).
68. M. Idir et al., "A 2D high accuracy slope measuring system based on a stitching Shack Hartmann optical head," *Opt. Exp.* **22**(3), 2770–2781 (2014).
69. S. C. Irick and W. R. McKinney, "Measurement of diffraction grating with a long trace profiler with application for synchrotron beamline gratings," in *AIP Conf. Proc.*, Vol. 417, pp. 118–121 (1997). ISSN:0094-243X
70. D. Cocco, G. Sostero, and M. Zangrando, "Technique for measuring the groove density of diffraction gratings using the long trace profiler," *Rev. Sci. Instrum.* **74**(7), 3544–3548 (2003).
71. J. Lim and S. Rah, "Technique for measuring the groove density of a diffraction grating with elimination of the eccentricity effect," *Rev. Sci. Instrum.* **75**(3), 780–782 (2004).
72. M. Thomasset, S. Brochet, and F. Polack, "Latest metrology results with the SOLEIL synchrotron LTP," *Proc. SPIE* **5921**, 592102 (2005).
73. B. Liu et al., "Measurement of groove density for concave gratings with the long trace profiler," *Rev. Sci. Instrum.* **77**(4), 046106 (2006).
74. V. V. Yashchuk et al., "Proposal for a universal test mirror for characterization of slope measuring instruments," *Proc. SPIE* **6704**, 67040A (2007).
75. V. V. Yashchuk et al., "High precision tilting stage as a key element of universal test mirror for characterization and calibration of slope measuring instruments," in *Abstract to The International Workshop on Metrology for X-ray Optics, Mirror Design, and Fabrication, Satellite Workshop at the 12th International Conference on Synchrotron Radiation Instrumentation, SRI 2018*, Berkeley (2015).

Valeriy V. Yashchuk is leading the X-Ray Optics Laboratory at the Advanced Light Source, LBNL. He received his MS degree in physics from St. Petersburg State University (Russia) in 1979 and his PhD degree from St. Petersburg Nuclear Physics Institute (Russia) in 1995. He has authored more than 160 research publications in the fields of atomic physics, nonlinear optics, electro- and magneto-optics, experimental scientific methods and instrumentation, and optical metrology. He is a member of SPIE.

Nikolay A. Artemiev graduated from the Department of Quantum Electronics of the Moscow Engineering-Physical Institute in 1993. His PhD thesis in physics, "Study of diffractive-refractive x-ray optics," was accomplished at Charles University in Prague in 2003. He is the author of more than 70 research papers. His main scientific interests are related with x-ray optics for conventional and synchrotron radiation sources and free-electron lasers. He is a member of SPIE.

Ian Lacey is a postbaccalaureate fellow at the X-Ray Optics Lab of Lawrence Berkeley National Laboratory's Advanced Light Source. He applies his mechanical and design background to improve instrumentation for characterizing and optimizing x-ray optics. He received his physics degree from California State University—East Bay, where collaborating with the Budker group, he conducted precision atomic spectroscopy experiments to test fundamental physics; presenting research findings at multiple national conferences. He is a member of SPIE.

Wayne R. McKinney received his PhD from Johns Hopkins in 1974. He received his postdoc at BNL and designed optical systems for the NSLS. In 1979, he worked in Richardson Gratings in Rochester New York and as an R&D manager in 1981. In 1987, he joined CXRO, working on components and designs for the ALS. He received Tech Transfer Awards and became an OSA fellow. His interests are first ALS infrared beamline and the first ALS spherical grating monochromator, optical calculation and metrology, particularly the adjustment of bendable x-ray optics. He now teaches at Diablo Valley College.

Howard A. Padmore is division deputy for experimental systems at the ALS, a third-generation source of synchrotron x-rays at Lawrence Berkeley National Laboratory. He received his BSc and PhD from the University of Leicester in the UK in 1977 and 1983, respectively. He is the author of over 200 research papers and formerly a co-editor of *Journal of Physics E: Scientific Instruments* and *Journal of Synchrotron Radiation*. He is a fellow of the APS, a fellow of the OSA, and winner of the 2013 Nerken prize of the AVS.